CHAPTER 3

DIRECT INTERFACING CIRCUIT BASED E-NOSE

3.0. Introduction

The pioneering work of interfacing sensors directly to digital embedded systems without intervening an analog-to-digital converters (ADC) was proposed in mid-1990s [2], where the efficacy of this measurement method has been established. Due to relatively simple design, compactness, low power consumption and low-cost of the acquisition system they have been deployed to address various sensor applications. Typically two classes of measurement techniques are documented in literature for direct interface of analog sensors to digital embedded system, one is direct sensor-to-controller which focuses on passive sensors (such as, resistive [2, 3, 9, 10, 12, 13, 19], capacitive [9, 14, 17], differential resistive [15], differential capacitive [16], resistive bridge sensors [6, 18] and inductive sensors[8]). The other class is direct analog-to-controller which focuses on sensors with analog voltage output [11]. DIC with various topologies have achieved success in measurement of responses obtained from resistive, capacitive and inductive sensors, but their investigation are mostly limited to a single sensor only. Moreover, such attempts do not cover classification paradigms using sensor arrays. Thus the procreation of a direct-interface circuit for a sensor array would be an useful tool for sensor measurement systems.

Typically when analog output of a sensor is fed to a µC, the voltage is digitized using an ADC. The output of the ADC is then processed in the microcontroller unit (MCU) for further analysis. But the analog output measurement system can be minimized by directly interfacing the sensors to the MCU without using the intermediate ADC.

As discussed in chapter 1, such analog voltage measurement circuits are remarkable in terms of performance considering their design simplicity. Analog voltage measurement using DIC was first demonstrated by Peter et al. [11] in a PIC 16CXX µC. They demonstrated that DI circuit has advantages in terms of both cost and power consumption. Due to this, the system was later replicated in different µCs for wide variety of sensors for measurement of analog voltage. Among them the most prominent designs were implemented in HC9S08Rx µC [20]; ST7FLITE05 (09) µC to study passive infrared (PIR) sensor responses [7]; and MSP430 µC by interfacing a separate sigma-delta modulator-AD 7400 [22]. The analog voltage in [7, 20, 22] is measured by realizing a sigma delta ADC using simple local hardware (capacitor and resistors) by proper sequencing of the built-in timer and comparator module of the MCU. Although

this approach does not require any ADC, the quintessential need of comparator and timer modules to measure the analog voltage demands for a relatively advanced and expensive µC. Bengtsson in [1] demonstrated that by using only two I/O pins of the µC an RC circuit based DI circuit can effectively measure analog voltage. Where, the DI circuit requires only two resistances, a capacitor and the µC digital I/O pins to have Tri-state capability. The analog voltage (simulated signal from Agilent 33220A) is measured based on the charging/discharging time of a *RC* circuit. A counter value is assigned in the MCU and the counter is incremented or decremented based on the voltage to be measured. The counter output generated is proportional to the applied analog voltage. Although DI technique is adopted by various researchers to interface sensor analog output to the MCU, it is mainly concentrated on a single sensor. While sensor array interface by DI approach and its multivariate analysis remains relatively unexplored.

Therefore, this chapter focuses on application of a direct interface circuit (DIC) with µC for measurement of responses from an array of metal oxide semiconductor (MOS) gas sensors and evaluation of its performance.

Further, to demonstrate the discriminative capability of the system both supervised and unsupervised classification paradigms have been designed and validated. Moreover, the system is capable of real time discrimination of various gases through the Feed forward back propagation (FFBP) artificial neural network (ANN) programmed in the µC. The ANNs were tuned to the optimal parameters and the system shows excellent recognition rate up to 98.75 %. Although, we demonstrated the feasibility of the system by classifying four different gases, the system is flexible and could easily be trained to perform in situ online gas sensing applications.

3.1. Operating Principle

The operating principle of the DIC-based E-Nose is discussed in subsequent sections.

3.1.1. DIC based measurement

Fig. 3.1 shows the basic DIC for a resistive sensor with analog output voltage V_{RL} [1]. The circuit relies on measuring the charging/discharging time of the *RC* circuit by the MCU which depends on the analog voltage (V_{RL}) to be measured. The DIC for the MOS gas sensors shown in Fig.3.1 implies that the PIC MCU used (PIC 18F45K22) is configured with two digital I/O pins at High-Z inputs. The measurement of V_{RL} implicates

a number of steps that are discussed as follows. First, a counting variable is initiated with a starting value of N_0, and then the capacitor is charged to the input voltage V_{RL} by configuring digital I/O-pin D_0 and D_1 of the MCU as high-Z inputs. In the preceding step, the voltage across the capacitor (V_{CP}) is compared with input logic high level (V_{IH}) of the digital port D_1. The time intervals at which the counter value will be incremented and decremented are D_d and D_C respectively, which are prime factors of the DIC based system. The value of D_d and D_C of are predetermined and is discussed later in this section. If $V_{CP} \geq V_{IH}$, D_0 is reconfigured as digital output low and the capacitor will be discharged through resistance R_1 and N_0 is incremented at an interval of D_d until V_{CP} reaches input logic low level (V_{IL}) of the digital port D_1. When $V_{CP} < V_{IH}$, D_0 is reconfigured as digital output high and the capacitor charges, subsequently the counter value N_0 is decremented at the interval of D_C until V_{CP} is charged to V_{IH}.

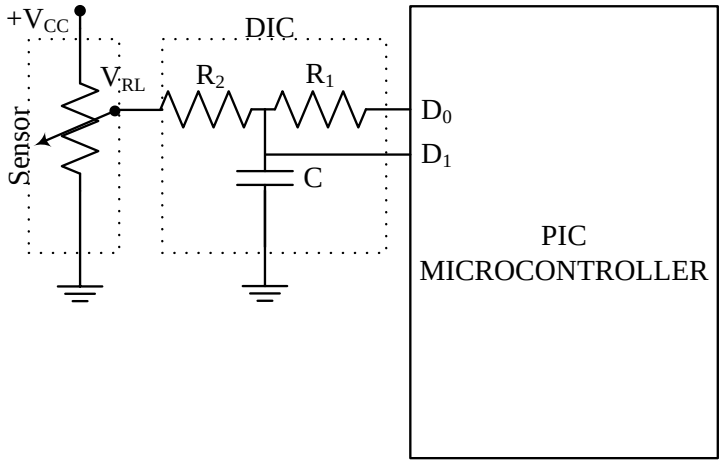

Fig. 3.1. Direct interfacing of sensor to MCU

The critical function of the system is to correctly measure the charging/discharging time to ensure reliable representation of V_{RL}, which can be achieved by precise measurement of parameters of components such as- resistances (R_1 and R_2); capacitor (C); input logic high (V_{IH}) and input logic low (V_{IL}) of the digital ports; supply voltage (V_{DD}) and oscillator frequency (F_0) [1]. We have measured the hardware components by a precision multimeter (Keithley-2110) which were found as- $C = 2.225\ \mu\text{F}$, $R_1 = 3.1979\ \text{K}\Omega$ and $R_2 = 9.861\ \text{K}\Omega$. The MCU used has specified low and high input/output logic levels and we have found the measured values as- $V_{IH} = 1.962\ \text{V}$, $V_{IL} = 1.880\ \text{V}$ and $V_{DD} = 4.65\ \text{V}$. Further the frequency of the local oscillator (F_0) of the

MCU was measured by a digital storage oscilloscope (DSO3202A) from Agilent Technologies and was found as 20 MHz. Although the value of V_{IL} should be near 1.6 V, however, we have obtained a slightly higher value of V_{IL} which is presumably due to the interference of various components integrated into the demo board. Moreover, V_{IL} may vary from µC to µC even for the same product.

The quantities of interest for DIC are calculated which includes, maximum charging time ($t_{c,\max}$) and maximum discharging time ($t_{d,\max}$) of the capacitor; starting counter value (N_0); delay to be provided in the program while charging (D_C) and discharging (D_d) [1]. Here we have aimed to achieve a 12-bit resolution, so the counter value is effectively set in the range of 0-4095. We have used 12-bit resolution which is sufficient to measure the smallest sensor voltage level at baseline (0.1 V - 0.4 V) for the MOS sensors. With this resolution, the 1LSB value accounts for $V_{DD}/2^{12}$, which is approximately 1 mV and sufficient for the minimum baseline voltages.

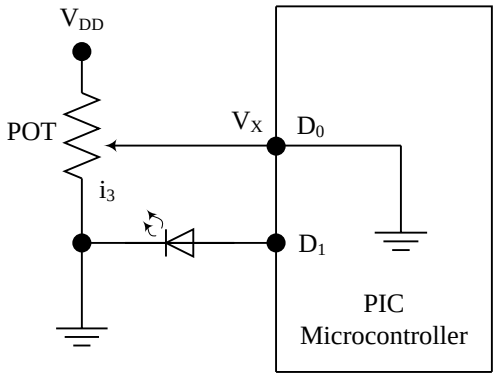

Fig. 3.2. Circuit for measurement of V_{IH} and V_{IL}

The measurement of V_{IH} and V_{IL} was accomplished by measuring the voltage V_X in the circuit shown in Fig. 3.2, using a high precision multimeter. In doing so, pin D_0 and pin D_1 is configured as input as output respectively and then an infinite loop is created in the code in order to execute: pin D_1 = pin D_0. V_X is measured and set at 0 V by tuning the potentiometer. V_{IH} is estimated by increasing the voltage across pin D_0 by carefully fine tuning the potentiometer. The minimum voltage across V_X at which the LED turns on is V_{IH}. Similarly, V_X is measured and set at V_{DD} by tuning the potentiometer. Now, V_{IL} is estimated by decreasing the voltage across pin D_0 by carefully fine tuning the potentiometer. The maximum voltage across V_X at which the LED turns off is V_{IL}.

Let us consider C is charged to a voltage $\geq V_{IH}$. Therefore, the capacitor will discharge until V_{CP} reaches V_{IL} . The simplified circuit model during discharge is depicted in Fig. 3.3.

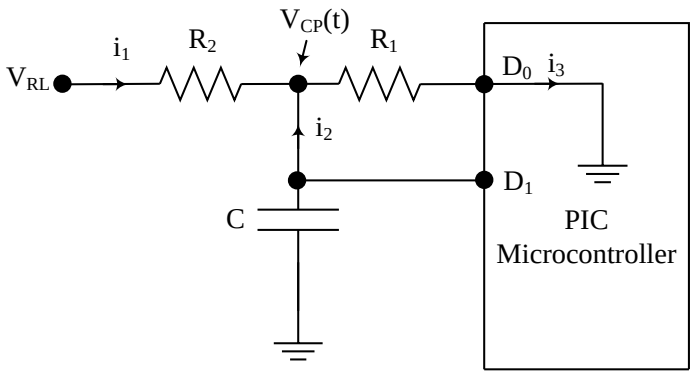

Fig. 3.3. Discharging circuit model

Now, from Fig. 3.3 we have:

$$\begin{aligned} & i_1 + i_2 = i_3 \\ & \frac{V_{RL} - V_{CP}(t)}{R_2} - C\frac{d}{dt}V_{CP}(t) = \frac{V_{CP}(t)}{R_1} \\ & \frac{d}{dt}V_{CP}(t) + \frac{1}{C}\left(\frac{1}{R_1} + \frac{1}{R_2}\right)\cdot V_{CP}(t) = \frac{V_{RL}}{C.R_2} \end{aligned} \tag{3.1}$$

The solution of the above first order differential equation is given by:

$$V_{CP}(t) = \frac{R_1}{R_1 + R_2}V_{RL} + V_0.e^{-\left(\frac{1}{c}\right)\left(\left(\frac{1}{R_1}\right)+\left(\frac{1}{R_2}\right)\right)\cdot t} \tag{3.2}$$

Again, $V_{CP}(0) = V_{RL}$ therefore V_0 can be easily determined as:

$$\begin{aligned} & V_{RL} = \frac{R_1}{R_1 + R_2}.V_{RL} + V_0 \\ & \Rightarrow V_0 = \frac{R_2}{R_1 + R_2}.V_{RL} \end{aligned} \tag{3.3}$$

Now, putting the value of V_0 in equation (3.1) we get:

$$V_{CP}(t) = \frac{V_{RL}}{R_1 + R_2}\left(R_1 + R_2.e^{-\left(\frac{1}{c}\right)\left(\left(\frac{1}{R_1}\right)+\left(\frac{1}{R_2}\right)\right)\cdot t}\right)$$

When $V_{CP}(t)$ reaches the input logic low i.e. V_{IL} in time t_d then:

$$t_d = -\frac{1}{(1/C)\times((1/R_1)+(1/R_2))}\times \ln\left(\frac{1}{R_2}\left(\frac{V_{IL}\cdot(R_1+R_2)}{V_{RL}} - R_1\right)\right) \qquad (3.4)$$

Similarly, when C is charged to a voltage $< V_{IH}$ the capacitor will charge until V_{CP} reaches V_{IH}. The simplified circuit model during charging is depicted in Fig. 3.4.

Now, from Fig. 3.4 we have:

$$i_2 + i_3 = i_1$$

$$\frac{V_{CP}(t) - V_{RL}}{R_2} - C\frac{d}{dt}V_{CP}(t) = \frac{V_{DD} - V_{CP}(t)}{R_1}$$

$$\frac{d}{dt}\left(V_{CP}(t) - \frac{1}{C}\left(\frac{1}{R_1}+\frac{1}{R_2}\right)\right)\cdot V_{CP}(t) = \frac{1}{C}\cdot\left(\frac{V_{DD}}{R_1}+\frac{V_{RL}}{R_2}\right)$$

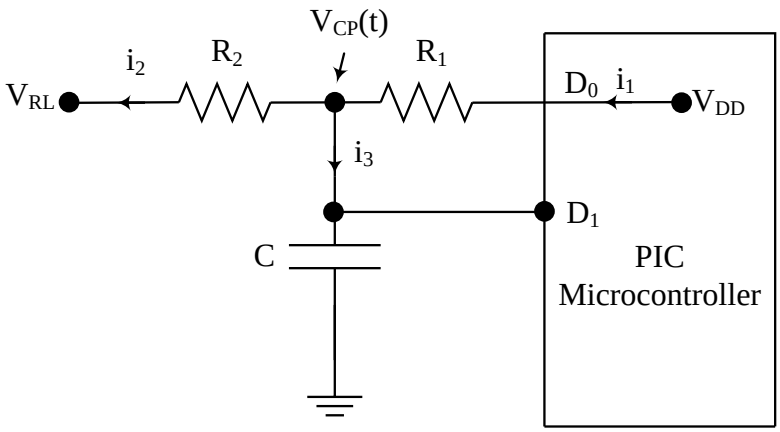

Fig. 3.4. Charging circuit model

The solution of the above first order differential equation is given by:

$$V_{CP}(t) = \frac{(V_{DD}/R_1)+(V_{RL}/R_2)}{(1/R_1)+(1/R_2)} + V_0.e^{-\left(\frac{1}{c}\right)\left(\left(\frac{1}{R_1}\right)+\left(\frac{1}{R_2}\right)\right)\cdot t}$$

$$= \frac{V_{DD}\cdot R_2 + V_{RL}\cdot R_1}{R_1+R_2} + V_0.e^{-\left(\frac{1}{c}\right)\left(\left(\frac{1}{R_1}\right)+\left(\frac{1}{R_2}\right)\right)\cdot t} \qquad (3.5)$$

Again, $V_{CP}(0) = V_{RL}$ therefore V_0 can be easily determined as:

$$V_{RL} = \frac{V_{DD}\cdot R_2 + V_{RL}\cdot R_1}{R_1+R_2}. + V_0$$

$$\Rightarrow V_0 = \frac{R_2}{R_1+R_2}.(V_{RL} - V_{DD})$$

Now, putting the value of V_0 in equation (3.5) we get:

$$V_{RL} \Rightarrow V_{CP}(t) = \frac{R_2}{R_1 + R_2} \cdot V_{DD} + \frac{R_1}{R_1 + R_2} \cdot V_{RL} + \frac{R_2}{R_1 + R_2}(V_{RL} - V_{DD}) \cdot e^{-\left(\frac{1}{c}\right)\left(\left(\frac{1}{R_1}\right)+\left(\frac{1}{R_2}\right)\right)\cdot t}$$

$$V_{RL} = \frac{R_2}{R_1 + R_2} \cdot V_{DD}(1 - e^{-\left(\frac{1}{c}\right)\left(\left(\frac{1}{R_1}\right)+\left(\frac{1}{R_2}\right)\right)\cdot t}) + \frac{V_{RL}}{R_1 + R_2} \cdot (R1 + R2 \cdot e^{-\left(\frac{1}{c}\right)\left(\left(\frac{1}{R_1}\right)+\left(\frac{1}{R_2}\right)\right)\cdot t}) \tag{3.6}$$

Now,When $V_{CP}(t)$ reaches the input logic high threshold i.e. V_{IH} in time t_c then:

$$t_c = -\frac{1}{(1/C) \times ((1/R_1) + (1/R_2))} \cdot \ln\left(\frac{V_{IH}(R_1 + R_2) - R_2 \cdot V_{DD} - R_1 \cdot V_{RL}}{R2 \times (V_{RL} - V_{DD})}\right) \tag{3.7}$$

The values of $t_{d,\max}$ and $t_{c,\max}$ were determined using (3.4) and (3.7) and setting $V_{RL} = V_{DD}$ and $V_{RL} = 0$, which were found to be 8.5 ms and 4.5 ms respectively.

The value of N_0 was determined by using (3.8) and found as 1412.

$$N_0 = \frac{t_{c,\max}}{t_{c,\max} + t_{d,\max}} \times 2^{12} \tag{3.8}$$

The delay to be provided to achieve full increment or decrement of N_0 to $t_{c,\max}$ and $t_{d,\max}$ during charging (D_C) and discharging (D_d) is subsequently calculated from (3.9) and (3.10) [1] respectively.

$$D_d = \frac{F_0 \times t_{d,\max}}{4 \times \left(2^{12} - N_0\right)} - 9 \tag{3.9}$$

$$D_d = \frac{F_0 \times t_{c,\max}}{4 \times N_0} - 9 \tag{3.10}$$

With $t_{d,\max} = 8.5\,\text{ms}$, $t_{c,\max} = 4.5\,\text{ms}$, $F_0 = 20$ MHz, and $N_0 = 1412$, the value of D_c and D_d are both found to be 7 instruction cycles. It is noteworthy to mention herein that the parameters D_c and D_d must be ≥ 0. The counter value depends on V_{RL}, and in worst case $V_{RL} = V_{DD}$ and the counter value is to be incremented from N_0 to $2^{12} - 1$. The DIC sampling time is the time taken for charging and discharging of the capacitor and the maximum value is 13 ms. The measurement time for the DIC includes the maximum charging/discharging time, delays and the processing of the µC. In our system the total measurement time is 13.0094 ms which includes 13 ms and 47 instruction cycles, where

one instruction cycle takes 200 ns ($4/(20\times10^6)$) using a 20 MHz crystal oscillator. Before interfacing the MOS sensor array to the MCU the DIC was calibrated by a simulated analog voltage obtained from a power supply (Agilent E361A) having a high voltage regulation and accuracy.

As discussed in previous section DIC have two approaches for sensors- one measurement of resistance and the other sensor voltage. In [12], the measurement of resistance technique is adopted to determine the resistance of RTDs (Pt-1000) while the methodology proposed in [1] addresses measurement of sensor response voltage. Moreover, the MOS gas sensor circuit recommended by manufacturer includes a load resistance (R_L) in series with the sensor, therefore the method discussed in [1] is more compatible for our proposed technique. Additionally, in traditional approaches MOS gas sensor based E-Nose commonly uses the response voltage as the feature, therefore we have adopted measurement of response voltage (V_{RL}) which is similar to conversion of analog voltage by ADC. The main advantages of the adopted technique are that the DIC circuit requires only two I/O-pins having Tri-state capability and it does not require any comparator or capture module either embedded or external. Due to these advantages DIC based sensor systems are explored to save μCs computation time for ADC operation. In view of this a multisensory framework has been used in DIC mode which can save a good number of components for large array (such as 16-32 size of array). Besides it is more compatible and it can be directly interfaced to inherent digital systems like CPLDs and FPGAs.

3.2. Sensor Interfacing and Data Acquisition

As mentioned in chapter 1, to validate the multisensory direct interface methodology, an E-Nose array consisting of three commercial MOS gas sensors has been chosen for direct interfacing of the sensors to a low cost μC and thereby classifies four different chemicals. In the subsequent sub-sections, detailed analysis of the DIC for multisensory measurement is presented.

3.2.1.MOS gas sensors

Commercial MOS gas sensors (Figaro) consists of an electrically heated ceramic pallet on which a thin film of n-type SnO_2 doped with a metal is deposited. The sensor supply voltage (V_C) and heater voltage V_H were supplied by a 5 V regulated power supply (SCIENTECH ST4072, 5 V, 1 A) as specified by the manufacturer to avoid any

instability while operating. The sensors take about 15 minutes to warm up and stabilize the output voltage level referred to as baseline voltage level. The room temperature and humidity during the experiments were maintained at 25 ℃ and $60 \pm 5\%$ respectively.

The basic principle of the gas sensor is chemisorptions which have been discussed in chapter 1. During the interaction of the sensing material with gas molecules, the conductance of gas sensor increases and a steady-state is reached. When the gas is removed the gas molecules dissociates from the sensing material without altering its structure and the sensor response returns to its baseline value. The time required to reach the steady-state value on exposure to gas is termed as 'sensing time' while the time to reach the baseline on removal of gas is termed as 'purging time'.

The output voltage (V_{RL}) across the load resistance (R_L) in Fig. 3.5 is proportional to the sensor resistance R_S is given by:

$$V_{RL} = \frac{V_C \times R_L}{R_S + R_L} \tag{3.11}$$

where, V_C is the supply voltage to the sensor. The sensitivity of the gas sensor can be calculated as,

$$S = \frac{R_a - R_g}{R_g} = \frac{\nabla R_g}{R_g} \tag{3.12}$$

where, R_a and R_g are the stable sensor resistances when exposed to air and gas respectively. Here equation (3.11) is valid when the digital ports of the µC are in high-Z.

3.2.2.Interface circuit

The direct interface MOS gas sensor based E-Nose is shown in Fig. 3.5. The three sensor responses V_{RL1}, V_{RL2} and V_{RL3} are interfaced to the MCU digital I/O pins (D_0, D_1), (D_2, D_3) and (D_4, D_5) respectively. In Fig. 3.1, we have shown the basic circuit of DIC interface to MCU. Here the resistive sensor is represented by a variable resistance producing a voltage V_{RL} interfaced to DIC.

In Fig. 3.5 we have replaced the variable resistance of Fig. 3.1 by the MOS gas sensor voltage divider circuit comprising the sensor (R_S) and a fixed resistor (R_L). This is done as per the design guidelines recommended in the sensors datasheets, such that any change in sensor resistance (e.g. R_{S1}) can be measured in terms of voltage drop across R_{L1}.

The voltage divider has certain effects on DIC measurement for instance the time constant of the system changes from $R_2 \cdot C$ to $((R_S \parallel R_L) + R_2) \times C$. However, we are concerned at measuring the voltage at the point V_{RL} using the circuit in Fig. 3.1, so similar conditions were assumed as proposed in [1].

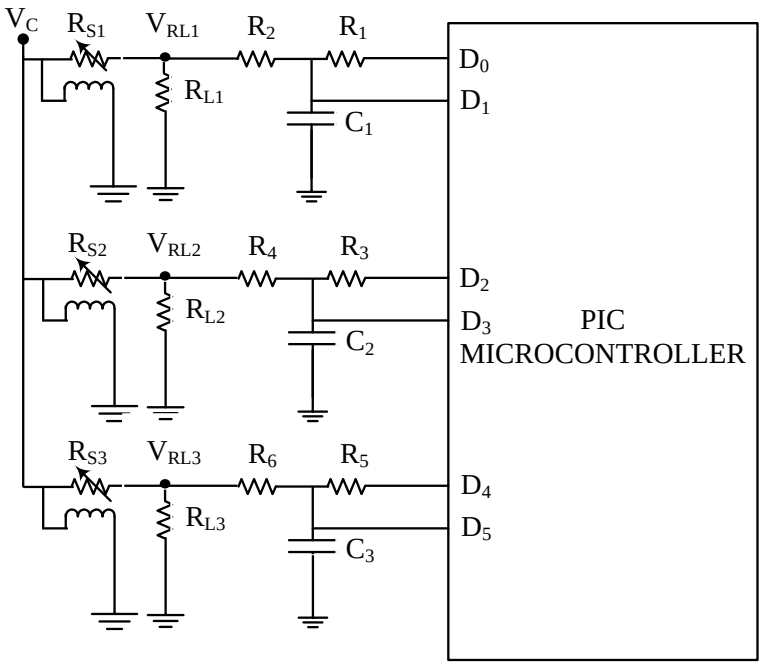

Fig. 3.5. MOS gas sensor array interfaced to the MCU (without amplifier)

In Fig. 3.5, V_{RL} is measured by using a voltage divider equivalent to that of the voltage divider network comprising the sensor. A variable resistance corresponding to that of the sensor is used to change the input voltage to be measured. The experimental observations indicate that, when $V_{CP} \geq V_{IH}$ the system has a very little affect on the discharge cycle and the value of N_0 almost remains the same. However, when $V_{CP} < V_{IH}$ and the capacitor is to be charged there is a small amount of voltage drop across the voltage divider, which in turn causes a slight increase in the value of N_0. The detailed analysis is shown in section 4.

Further it is observed experimentally that the output response of the sensors is in the range of $0 - V_{IL}$. Therefore, to validate our systems measurement capability for both the cases (i.e. $V_{CP} < V_{IH}$ and $V_{CP} \geq V_{IH}$) the output response of the sensors are amplified in the range of $0 - V_{DD}$ using a two stage inverting amplifier and subsequently measurement is performed using the proposed circuit (Fig. 3.6).

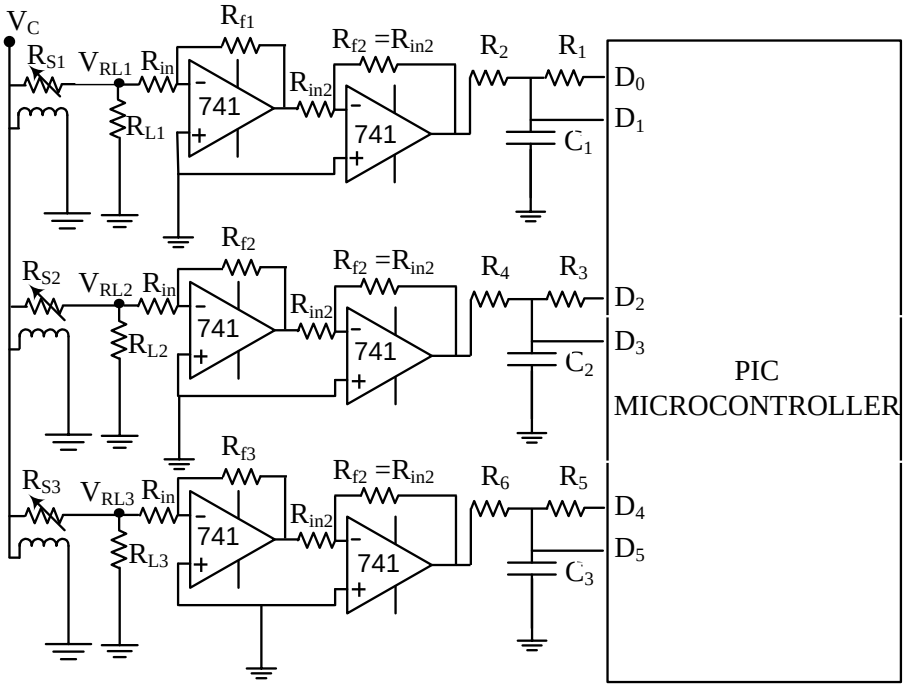

Fig. 3.6. MOS gas sensor array interfaced to the MCU (amplifier included)

3.2.3.Measurement technique

To study the sensor dynamics which gives us the information about the important parameters i.e. sensing and purging time, we first interfaced the sensor output terminals to a PC via a DAQ card (NI USB-6211) and Lab VIEW. The sensor array is then exposed to gas samples, which converts the gas concentration to proportionate measurable electrical voltage, which is captured and stored in the computer. The optimum sensing and purging time were found as 80 s and 100 s respectively.

The MCU based data acquisition is performed through direct analog-to-controller method. Fig. 3.7 shows the flowchart of the algorithm implemented in the MCU to measure the count values corresponding to the sensor responses V_{RL1}, V_{RL2} and V_{RL3}. We also evaluate how accurately different gases are classified using the proposed multi-sensory measurement method. In doing so, Principal component analysis (PCA) is computed in MATLAB to observe the clusters formed by the gas sensors to different gases. After PCA, Feed Forward Back Propagation (FFBP) artificial neural network (ANN) is modeled in MATLAB, which acts as decisive factors to determine how accurately the gases are classified [23-25]. We have determined the performance parameters of the ANN like weights, biases, number of hidden neurons etc. We have chosen FFBP since it is relatively simple and can effectively represent multi-class

recognition tasks [5]. The performance parameters are then used to simulate the ANN in the μC through embedded C programming to identify different gases.

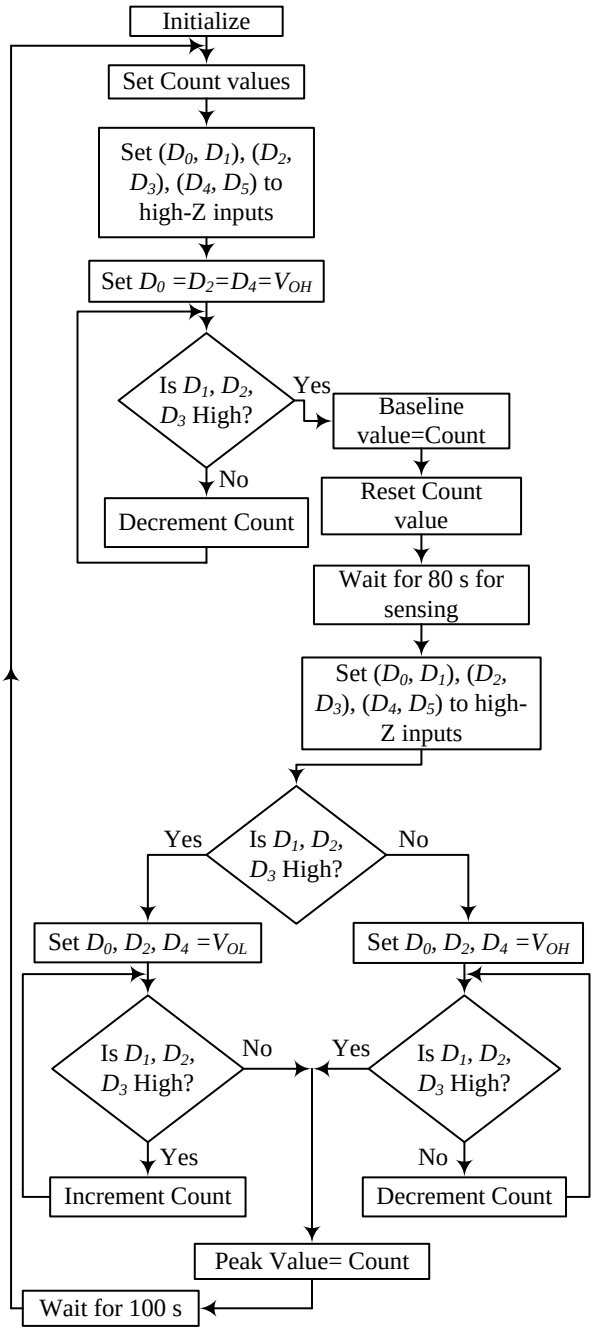

Fig. 3.7. Algorithm for analog voltage measurement of three gas sensors

When the sensor response is at baseline value the output voltage V_B is always less than V_{IH}, the counter value at baseline is measured by charging the capacitor to V_{IH} and decrementing the counter from N_0 (Fig. 3.8). The capacitor is then fully discharged and the counter value is again initialized to N_0 to measure the stable peak sensing voltage. Again when the sensor response reaches the peak value V_P on exposure to gas it will be

either $V_P < V_{IH}$ or $V_P \geq V_{IH}$. If $V_P < V_{IH}$ then similar to baseline measurement the capacitor is charged to V_{IH} and counter value is measured by decrementing N_0 as shown in Fig. 3.8. Similarly when $V_P \geq V_{IH}$ the capacitor is discharged to V_{IL} and the counter is incremented from N_0 as shown in Fig. 3.9. After measuring the peak value the capacitor is again fully discharged. While measuring the response from the sensor array, first the counter value at baseline is measured for the three sensors sequentially and then after reaching the sensing time the peak values are measured sequentially.

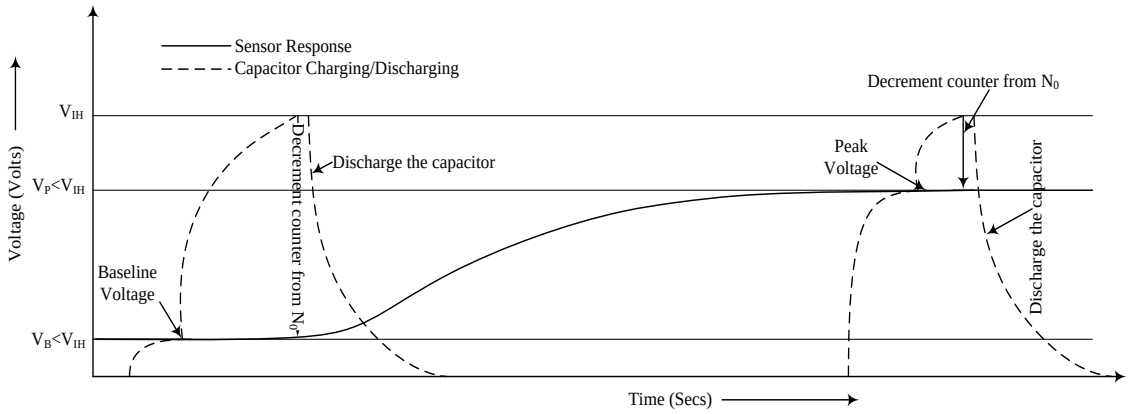

Fig. 3.8. Counter value measurement for peak and base when $V_P < V_{IH}$

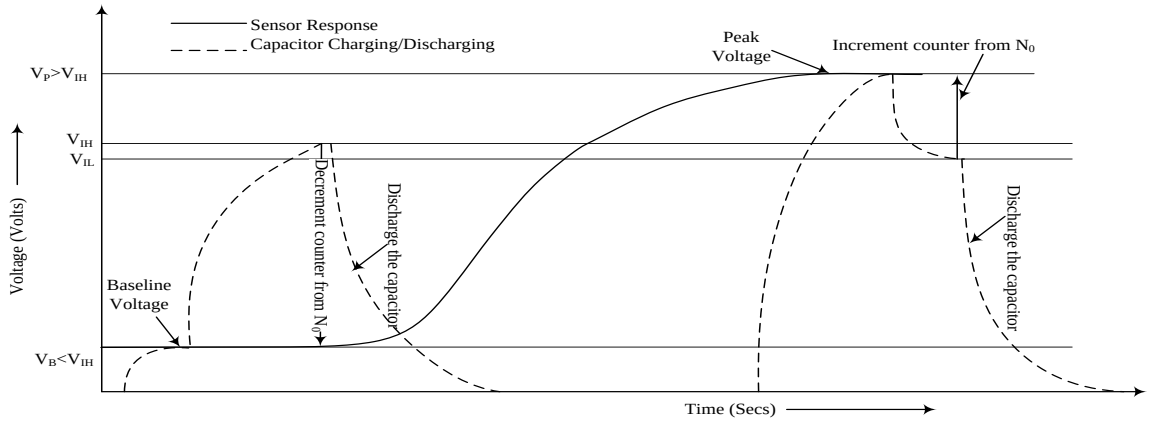

Fig. 3.9. Counter value measurement for peak and base when $V_P \geq V_{IH}$

The counter value corresponding to baseline and the peak of the sensors are stored in the memory of the MCU and transferred to a personal computer and stored as a data file. The count values corresponding to the baseline and peak value of the sensor response are used to extract the features using-

$$F_i = N_{P,i} - N_{B,i} \tag{3.13}$$

where, $N_{P,i}$ and $N_{B,i}$ are the count values corresponding to peak voltage (V_P) and baseline voltage (V_B) of the sensor. The count values measured was transferred to a PC through an asynchronous serial link at a baud rate of 9600.

3.3. Experimental Setup

The aim of this work is to directly interface multiple gas sensors in array mode to configure all the characteristics of an Electronic Nose. Metal oxide semiconductor (MOS) gas sensors from Figaro Inc. are most popular devices for developing E-Nose. We have selected three Figaro MOS sensors (TGS 2201, TGS 2620, and TGS 832) based on their selectivity and sensitivity to a wide range of gases.

Since the direct interface technique takes advantage of the change in resistance corresponding to one level of input to another level the change in resistance of the selected sensors on application of the gases are first studied. Fig. 3.10 shows the pictorial diagram of the experimental setup. We have used four ACS grade chemicals from Merck- methanol (G1), acetic acid (G2), acetone (G3) and 2-propanol (G4). The selected gases fall in the same group of the target gases of the selected sensors.

3.3.1.Sample Preparation

Since the objective of the direct interface E-Nose is to classify and discriminate between different gases, we attempt to activate the sensors to get considerably higher levels of response voltages. To do so, we have generated the gas analyte at higher concentration levels (100 ppm-200 ppm) compared to their minimum sensing levels of 40 ppm (TGS 2620) and 10 ppm (TGS 832/2201) respectively. This reduces the chance of getting lower response voltage or totally indiscriminative nature of signals. A 200 µL volume of each chemical sample was micropipetted into a sample chamber made of Borosil glass (280 ml) and stabilized for 10 minutes to obtain a concentration level which was calculated using equation (3.14) available in [21]-

$$C_n = \frac{V_{vap}}{V_{gc}} \times 10^6 \tag{3.14}$$

where, V_{gc} is total volume of the sensor chamber and the volume of gas vapor V_{vap} is given by,

$$V_{vap} = \frac{D_{liq} \times V_{liq}}{M} \times \frac{R \times T}{P} \tag{3.15}$$

where, D_{liq} = density of liquid (G1- 0.792 g/ml , G2- 1.049 g/ml , G3- 0.791 gm/ml and G4- 0.786 g/ml), R = gas constant (0.08206 g/mol), T = temperature (25 °C), P = pressure (0.0922 atm), M = molecular weight (G1- 32.04 g/mol , G2- 60.05 g/mol , G3- 58.05 g/mol and G4- 60.01 g/mol), V_{liq} = volume of liquid (200 µL), C_n = gas concentration in ppm.

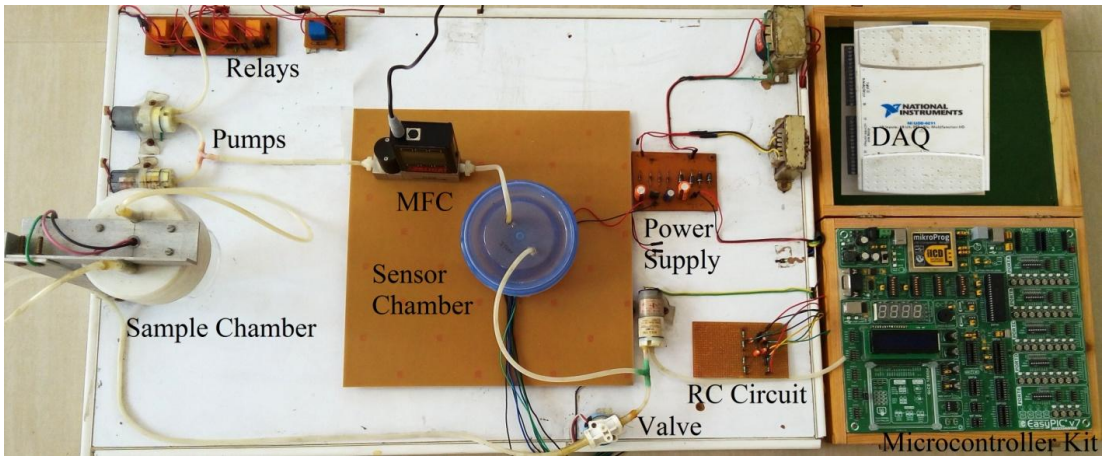

Fig. 3.10. Experimental E-Nose setup

The effective volume of the gas sensor chamber is found as 577 ml, including the volume of the pipes. The gas concentration was calculated using equation (3.14) and (3.15) and was found as- G1-211.21 ppm, G2-149.26 ppm, G3- 116.37 ppm, and G4-111.75 ppm. The gas was pumped to the sensor chamber at a flow rate of 1.2 SLPM controlled and regulated by a mass flow controller (Alicat MC-05 SLPM-D).

The PIC MCU we have used is a high performance RISC CPU based on advanced Harvard architecture. The MCU comprises of 40 pins having 32 kb of reprogrammable flash memory and 2 kb of RAM.

3.4. Experimental Results

The DI circuit was calibrated by measuring the counter value produced by applying analog input voltages from a precision power supply (Agilent E361A). The measurement is also repeated for the voltage divider network by varying the output resistance akin to the sensor circuit. The results of the counter values were stored in PC via a serial link through the MCU. Fig. 3.11 shows the calibration characteristics of the analog input voltages corresponding to the counter value estimated by the MCU.

After analyzing the DIC by applying analog voltages from a power supply and a voltage divider network values of which are equivalent to the sensor circuit, an

experiment was conducted to amplify the sensor responses to achieve the output response for methanol in the range of $0-V_{DD}$. However, variation of sensor response voltage similar to resistive network for calibration characteristics is not possible due to its random fluctuations. Therefore we have used the resistive network in place of the sensor for calibration characteristics.

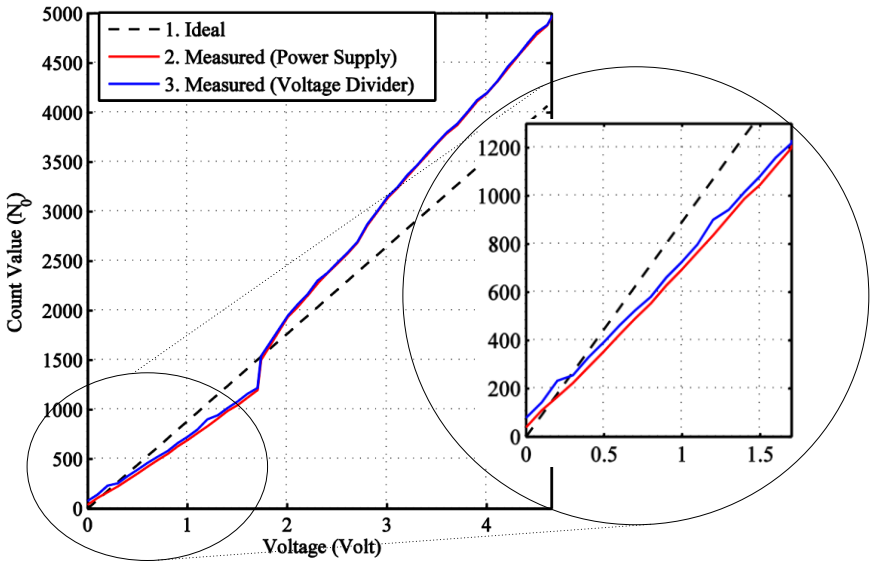

Fig. 3.11. Calibration Characteristics of the DIC

To perform real time gas classification, the DIC based gas sensor array was interfaced to the MCU and counter values were measured for four chemical gas samples. To form the feature matrix, we measure the counter value at the two response conditions of the output response - baseline and peak steady state. For each gas samples 50 times the measurements were repeated. Table 3.1 shows the lowest, mid and highest baseline sensor response voltages and peak sensor response voltages along with their corresponding count values for the tested gases. The sensor response pattern to different gases is depicted in Fig. 3.12.

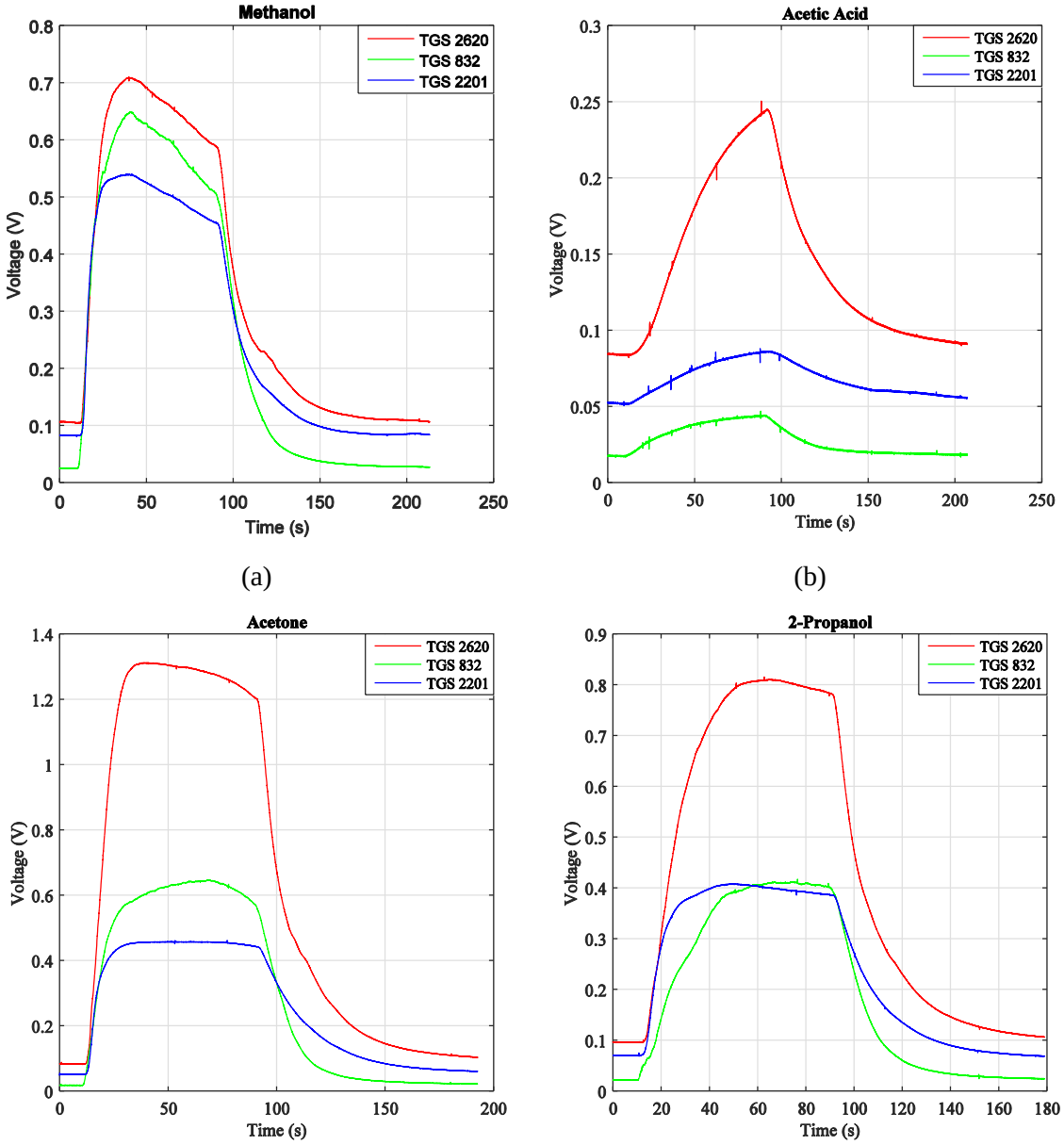

Fig. 3.12. Raw sensor responses to (a) Methanol (211.21 ppm), (b) Acetic Acid (149.26 ppm), (c) Acetone (116.37 ppm) and (d) 2-Propanol (111.75 ppm)

Fig. 3.13 depicts the actual and the amplified values of the sensors output responses which are measured by the DIC on exposure to methanol. The significant aftermaths of the measurement indicates that the system works fine for both the cases (i.e. $V_{CP} < V_{IH}$ and $V_{CP} \geq V_{IH}$).

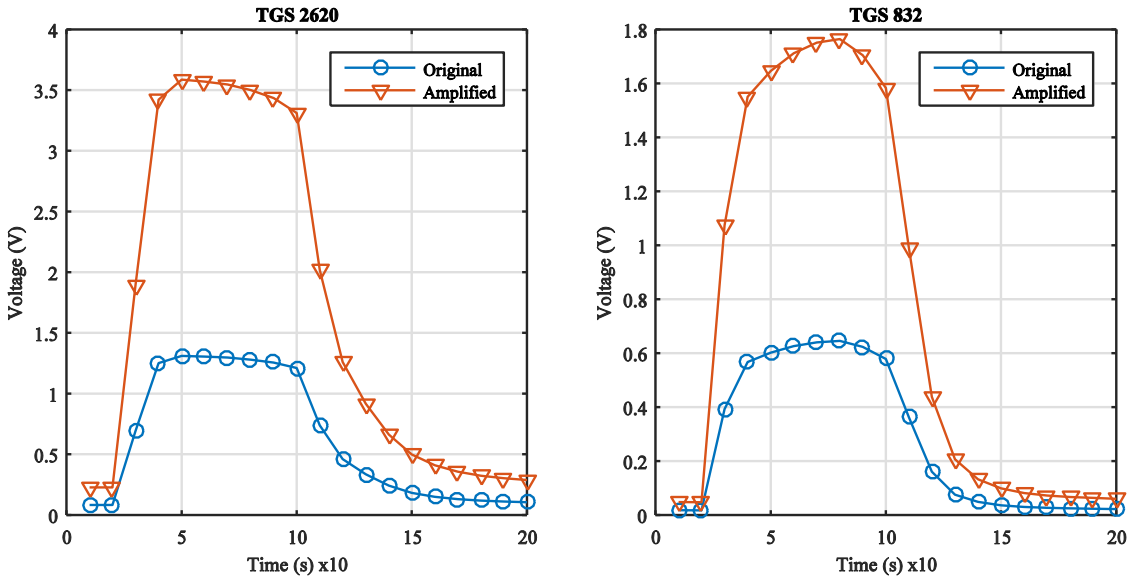

(a) (b)

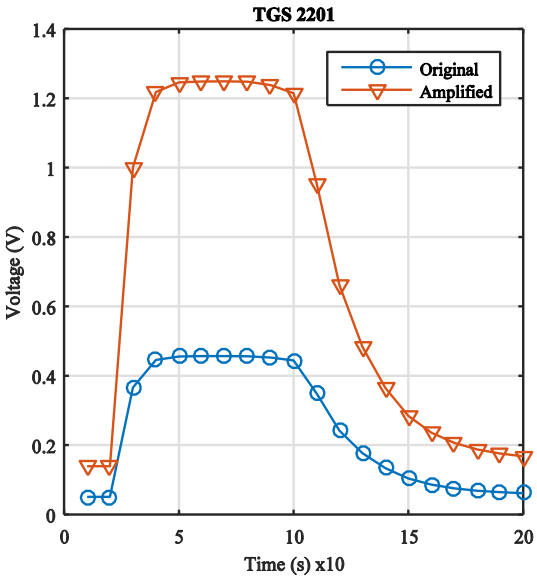

(c)

Fig. 3.13. Raw and amplified response of to methanol (211.21 ppm)

The mean and standard error mean (S.E.M) of the measured count values are shown in Table 3.2. For a total of 200 data each for baseline and response peak, the sensors resulted in a consistently stable response with a maximum S.E.M of ± 0.8211 and ± 17.1461 count value respectively. The feature dataset (baseline- n_b and peak- n_p) consists of a total of $4 \times 50 \times 3$ data, 200 for each sensor for four gases.

Table 3.1 Baseline Voltages of the three sensors along with their corresponding count values

Environment	TGS 2620		TGS 832		TGS 2210	
	Voltage (V)	Count Output (*N*)	Voltage (V)	Count Output (*N*)	Voltage (V)	Count Output (*N*)
Ambient air	0.22	186	0.15	147	0.27	221
	0.25	208	0.17	160	0.31	237
	0.28	228	0.20	174	0.34	253
Methanol	0.93	651	0.90	632	0.90	631
	1.07	752	1.07	754	0.99	698
	1.17	819	1.25	876	1.09	769
Acetic Acid	0.52	370	0.26	211	0.40	291
	0.50	419	0.32	244	0.44	318
	0.67	478	0.37	277	0.48	346
Acetone	0.97	680	0.55	392	0.66	471
	1.12	783	0.70	495	0.75	530
	1.39	979	0.98	688	0.84	589
2-Propanol	0.52	371	0.33	250	0.63	450
	0.76	538	0.47	339	0.73	518
	1.02	718	0.73	517	0.87	609

Before applying the data in ANN for gas classification the correlation of the direct-interface sensor responses was tested using PCA, which shows four distinct clusters of the four gases as shown in Fig. 3.14. The PCA expresses the feature patterns in terms of linear combination of orthogonal vectors, where each principal components (orthogonal vectors) account for variance in the feature set with decreasing degree of importance. Here, the first three principal components were used as they accounted for more than 99% of variance (Table 3.3). Therefore PCA validates that the measured counter values faithfully represents the sensor response voltages when exposed to gases.

Table 3.2 Estimate of counter values corresponding to baseline and peak responses of three gas sensors for four gases

Sensors	n_b	Baseline Mean ± S.E.M	n_p	Gas	Peak Mean ± S.E.M
TGS 2620	200	215.66 ± 0.61	200	G1	762.28 ± 6.00
				G2	411.68 ± 4.37
				G3	793.10 ± 13.98
				G4	576.20 ± 17.14
TGS 832	200	163.97 ± 0.40	200	G1	785.36 ± 8.87
				G2	234.10 ± 2.78
				G3	503.20 ± 13.53
				G4	384.58 ± 13.66
TGS 2201	200	238.62 ± 0.82	200	G1	713 ± 5.07
				G2	318.58 ± 1.85
				G3	543.08 ± 4.19
				G4	534.34 ± 7.46

Note: n_b, n_p are total count values estimated for baseline and peak respectively; S.E.M. = Standard error of mean

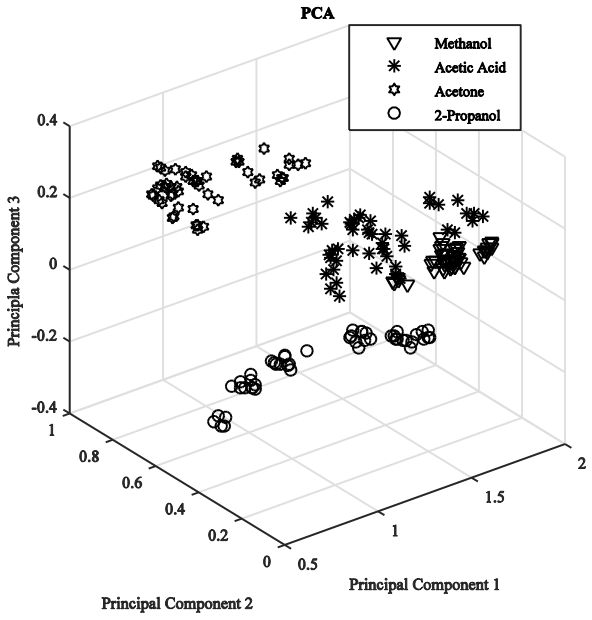

Fig. 3.14. PCA of the sensor responses

The feature data is used in an unsupervised classification algorithm- LDA where it models the difference between data class by maximizing the ratio of intra-class variance to the inter-class variance. The LDA based transformation of the feature data is used to generate a graphical 2-D plot to examine the cluster separation. It is observed that LDA forms four none overlapping and distinctive clusters of the four tested gases. The plot of LDA shown in Fig. 3.15 illustrates the relationship and trends of the E-Nose array to different gases.

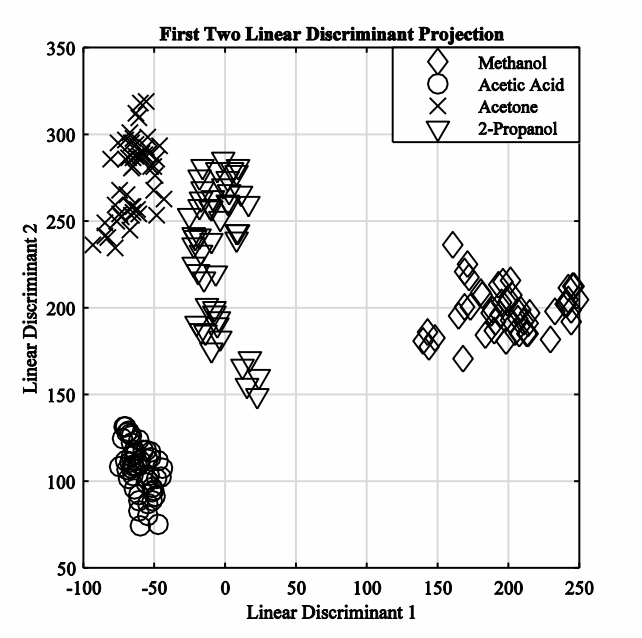

Fig. 3.15. LDA of the sensor responses

Table 3.3 Results of PCA

PC	% Variance	Eigenvalue	Principal Components		
			TGS 2620	TGS 832	TGS 2201
PC1	98.46	0.14802	0.6078	0.2855	0.7410
PC2	1.03	0.00155	0.7029	-0.6277	-0.3347
PC3	0.50	0.00075	0.3695	0.7242	-0.5822

The feature data of counter values were used in an ANN model. In this study the ANN modeling and performance was analyzed in two stages, modeling with software using MATLAB and coding in the PIC MCU. The modeling with software has three steps as shown in Fig. 3.16, at the first step the data set was partitioned for training and testing. The total dataset consists of $N_g \times N_f \times N_s$ $(4 \times 50 \times 3)$ where N_g is the number of gases = 4; N_f is the number of feature data = 50; and N_s is number of sensors = 3. The feature dataset was partitioned in the ratio of 60:40 (i.e. $360:240$) for training and testing. In second step ANN model is formed by varying the ANN parameters such as- number of hidden neurons (n), error goal, learning rate and activation function. The training parameters and performance of the optimal network is shown in Table 3.4 and Fig. 3.17 respectively. The simulation of the MATLAB program resulted in the following optimum training parameters- hidden neuron = 3, learning rate = 0.1, error goal $= 10^{-6}$, mean squared error (M.S.E.) $= 7.447 \times 10^{-7}$ and activation function *logsig* and *tansig* in

input and hidden layer respectively (Table 3.5). In the last step the weights, biases and training parameters were obtained from MATLAB.

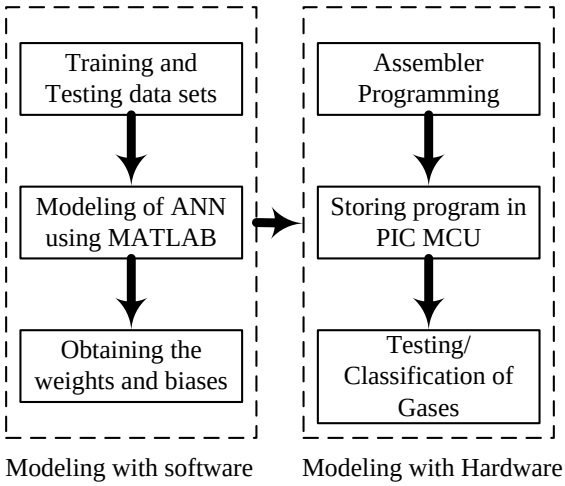

Fig. 3.16. Methodology for direct-interface of E-Nose

A total of 200 response data were gathered for training and testing (50 for each gas) and the ANN based classification parameters obtained from MATLAB simulation is shown in Table 3.6. After coding the ANN in MCU, on-line gas sensing was performed by direct-interfacing and classified the four gases by the interfaced E-Nose. The overall consumption of program memory is 8782 bytes and RAM memory is 142 bytes.

Table 3.4 ANN training parameters

Parameter	Initial Setting
The number of layers	3
The number of neuron on the layers	Input: 3, hidden: 1, 2 and 3, output: 1
The initial weights and biases	Random
Activation function	Tansig-Logsig-Purelin
Learning rule	Levenberg-Marquart backpropagation
Sum-squared error	0.000001

The weights and biases of the well trained network are shown in Table 3.5. The gas classification results of the direct interface E-Nose is shown in Table 3.7 and the ANN model output are found to be in the range of acceptable limits. Each gas was tested 20 times by the MCU and it is perceived from Table 3.7 that only one time 2-propanol is misidentified as methanol, and in rest of the cases the gases are classified accurately. Thus, direct interfacing based E-Nose system can find their place as an alternative to ADC based systems.

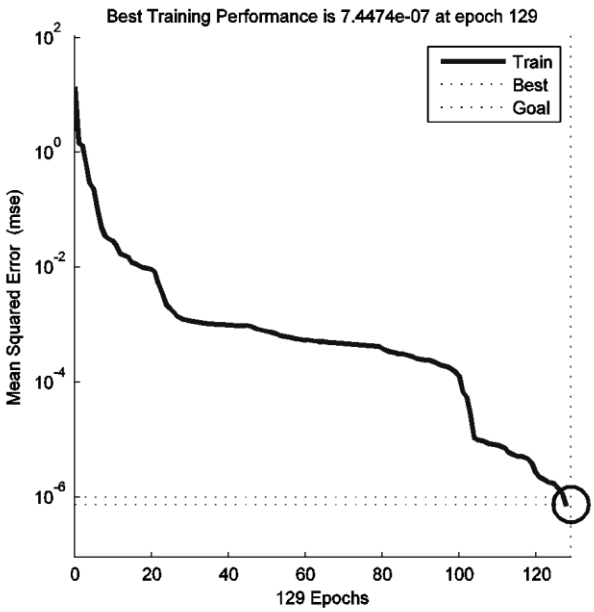

Fig.3.17. Performance function with $n = 3$

Table 3.5 ANN performance parameters

Data size	n	Computation time (s)	Epochs	Accuracy (%)	M.S.E.
$4 \times 50 \times 30$	1	11.024	1000	50	0.654
	2	2.726	134	50	0.862
	3	2.982	129	98.75	7.4×10^{-7}

Table 3.6 Weights and biases of the ANN

Parameter	Values
$IW\{1,1\}$	[1.5490 -2.2493 0.0058; 3.5414 0.6270 -5.4097; 0.0206 0.0102 -0.0051]
$LW\{2,1\}$	[2.7049 3.6246 -0.5834; -2.6624 -4.0444 0.9280; 7.9385 9.1743 -53.5227]
$LW\{3,2\}$	[-35.0128 -11.7103 3.0016]
$b1$	[-1.5276; -1.2542; -10.0409]
$b2$	[-7.8588; 6.9477; 60.1021]
$b3$	[12.7102]

Table 3.7 Performance of Gas Classification for direct-interface E-Nose

Gas	Sensor (TGS)	Measured count values	Equivalent peak voltage	Accuracy
Methanol	2620	600	0.8597	100%
	832	712	1.1178	
	2201	530	0.7512	
Acetic acid	2620	261	0.3518	100%
	832	112	0.1046	
	2201	116	0.1166	
Acetone	2620	683	0.9746	100%
	832	459	0.6514	
	2201	297	0.4109	
2-Propanol	2620	232	0.3033	95%
	832	121	0.1187	
	2201	211	0.3667	

3.4.1.Scalability Analysis

In order to perform scalability analysis new sets of data were recorded. In contrast to the previous experiments, the sensor array is exposed to a high concentration of the chemical analyte for which 300 μL of each chemical samples is injected into the sample vial.

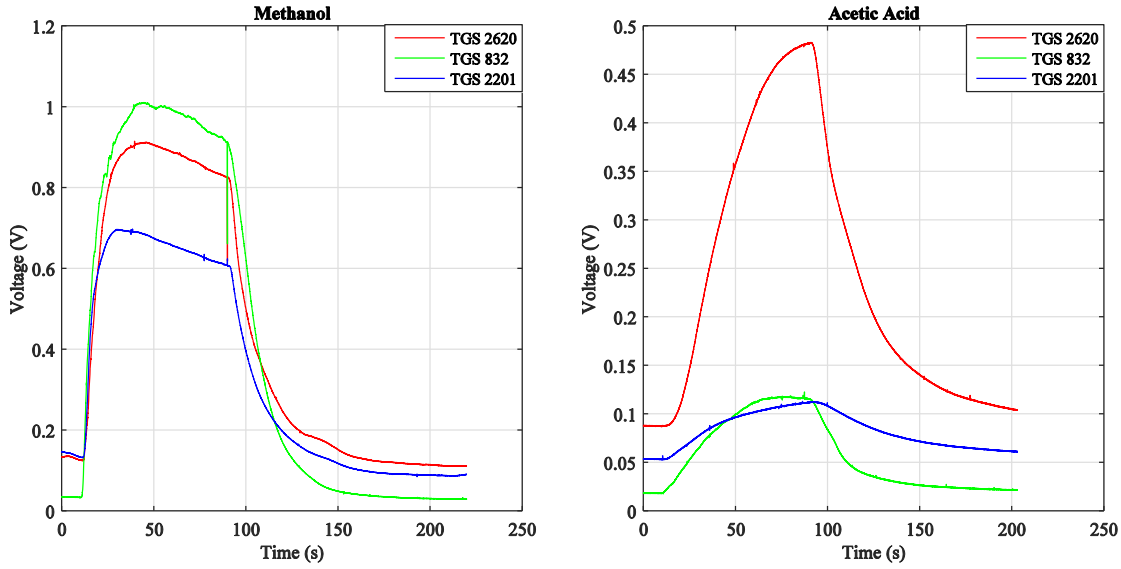

(a) (b)

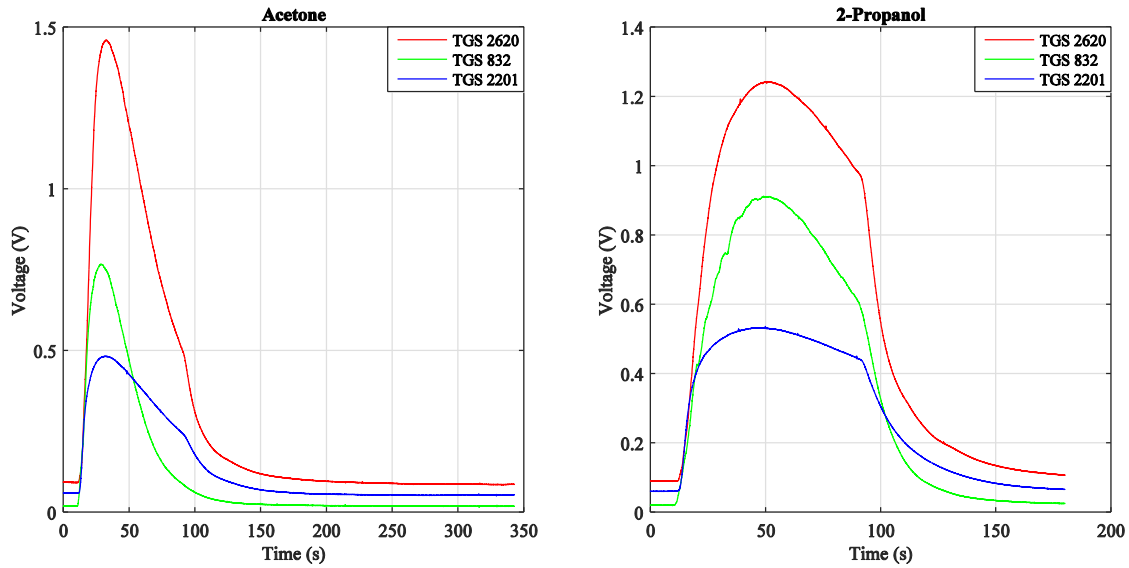

(c) (d)

Fig. 3.18. Raw sensor responses to (a) Methanol (316.82 ppm), (b) Acetic Acid (223.89 ppm), (c) Acetone (174.55 ppm) and (d) 2-Propanol (167.62)

The gas concentration was calculated using equation (3.14) and (3.15) and was found as- G1-316.82 ppm, G2-223.89 ppm, G3- 174.55 ppm, and G4- 167.62 ppm. The response characteristics of the sensor array to the different gases are shown in Fig. 3.18.

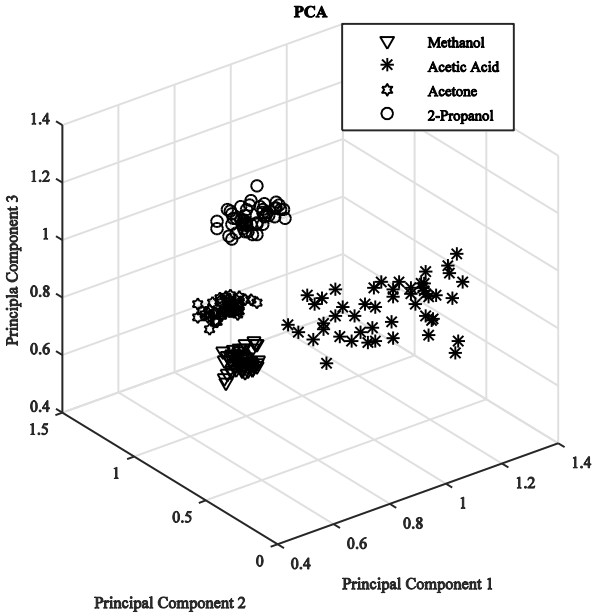

Fig. 3.19. PCA of new dataset (high ppm)

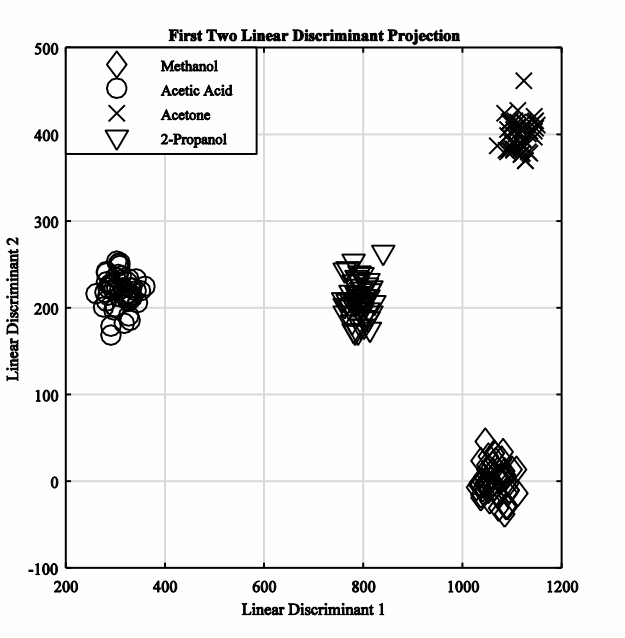

Fig. 3.20. LDA of new dataset (high ppm)

We first examine the change in counter value due to the change in the corresponding output voltage level of the sensors on exposure to different gases. In order to evaluate the effect of counter value on the gas sensing properties of the sensor array the previously used high purity chemicals (acetone, acetic acid, methanol and 2-propanol) were collected to conduct the experiments. PCA and LDA were performed to ensure cluster formation (shown in Fig. 3.19 and Fig. 3.20).

Since the PCA plot can only provide us a visual aid for observing the cluster separation a quantitative metric- inter-intra class distance ratio is measured to quantify the separation of clusters in a 3-D space. Therefore, the class distance metric between the PCA plots of Fig 3.14 and Fig. 3.19 obtained using 200 µL and 300 µL of gas volume is compared. The Euclidean intra-class distance (d_{intra}) for a particular gas cluster (Table 3.8) is determined by averaging the class distance among the entire samples of a cluster using (3.16):

$$d_{\text{intra}} = \sum_{i=1}^{n} \sqrt{X_i - \overline{X}} \Big/ N \qquad (3.16)$$

where, X_i is the value of the i^{th} sample of the cluster, $\overline{X}$ is the sample mean of the cluster and N is the total number of samples within that cluster.

The Euclidean inter class (d_{inter}) distance is measured by calculating the distance among the means of the various clusters using (3.17):

$$d_{\text{inter}} = \sqrt{\sum_{i=1}^{3}\left(\overline{X_{i1}} - \overline{X_{i2}}\right)^2} \tag{3.17}$$

where, $\overline{X_{i1}}$ is the sample mean of cluster of Gas 1, $\overline{X_{i2}}$ is the sample mean of cluster of Gas 2 and $i = 1{:}3$ represents the three PCA coordinates.

In our case we have analyzed four gas samples which give a total number of 12 possible combinations of inter class distance. Table 3.9 shows the Euclidean inter class distance between all the four gas clusters. We have further, determined the Euclidean inter-intra class distance ratio to obtain a single measure of class separation (Table 3.10) for all the classes using (3.18):

$$d_{ratio}(i, j) = \frac{d_{\text{inter}}(i, j)}{d_{\text{intra}}(i)} \tag{3.18}$$

Table 3.8 Euclidean intra class distance

Gas	200 µL	300 µL
Methanol (G1)	0.0938	0.0495
Acetic Acid (G2)	0.2242	0.2058
Acetone (G3)	0.2099	0.0507
Propanol (G4)	0.3569	0.0686

Table 3.9 Euclidean inter class distance for nADC and ADC

Volume	G1G2	G1G3	G1G4	G2G3	G2G4	G3G4
200 µL	0.3412	0.8624	0.5569	0.6335	0.4410	0.5696
300 µL	0.8692	0.2535	0.9914	0.7610	0.5795	0.7634

Table 3.10 Euclidean inter-intra class distance ratio for nADC and ADC

(a) 200 µL

	G1	G2	G3	G4
G1	0	3.6375	9.1940	5.9371
G2	1.5219	0	2.8256	1.9670
G3	4.1086	3.0276	0	2.7137
G4	1.5604	1.2356	1.5960	0

(b) 300 µL

	G1	G2	G3	G4
G1	0	17.5596	5.1192	20.0283
G2	4.2235	0	3.6978	2.8156
G3	4.9980	15.0099	0	15.0572
G4	14.4519	8.4475	11.1283	0

Table 3.11 Class distances of the entire dataset

Parameters	200 µL	300 µL
Average Inter-Class distance	0.5674	0.7029
Average Intra-Class distance	0.2212	0.09365
Inter-Class/Intra-Class distance ratio	2.565	7.50

It is observed from Table 3.8-3.11 that the average inter-class distance for low ppm is less than that of high ppm. It indicates that the gases are well separated for high ppm then low ppm. Moreover, the lower value of average intra-class distance for high ppm indicates that the data samples in a cluster are very close to each other. Further, the ratio of the inter-class and intra-class is higher for high ppm compared to that of low ppm. Therefore, the class separation of the different classes is more in case of high ppm.

3.4.2.ANN Performance

The dataset was divided for training and testing in the ratio of $60:40$ and a three layer FFBP ANN model was programmed in MATLAB with one hidden layer.

Table 3.12 ANN performance parameters with n=1, 2 and 3

Data size	Hidden neuron (n)	Computational time (s)	No. of epochs	Accuracy (%)	Mean squared error (M.S.E.)
$4\times50\times3$	1	16.64	590	50	1.0701
	2	10.37	1000	75	0.1250
	3	1.61	19	98.75	5.3×10^{-7}

The performance of the ANN was evaluated changing the number of hidden neurons to observe the performance. Then the optimal number of hidden neurons was found to be $n=3$ which gives highest classification accuracy of 98.75 %. Table 3.12 shows the performance parameter of the FFBP ANN with $n=1, 2, \text{and } 3$. The algorithm of the optimal FFBP model with $n=3$ is then coded in the µC to perform on-line gas discrimination by the DI based E-Nose. The result shows that the errors are within the range of acceptable limits.

For each gas 20 samples were used for online testing. The confusion matrix of the test results of the DIC based E-Nose is shown in Table 3.13 which informs about the individual class accuracy as well as overall class accuracy. Table 3.13 shows that the

developed DIC based E-Nose can successfully recognize the four tested gases. Moreover the µC utilizes only 9% RAM (142 bytes) and 27% ROM (8782 bytes), which makes it feasible to adopt the proposed methodology for low cost µCs. The scalability analysis reveals that the methodology performs effectively on new sets of data.

Table 3.13 Confusion matrix

		Predicted output				
		G1	G2	G3	G4	
Actual output	G1	20	0	0	0	100%
	G2	0	20	0	0	100%
	G3	0	0	20	0	100%
	G4	1	0	0	19	95%
		95.23%	100%	100%	100%	98.75%

3.5. Conclusion

This chapter addressed a protocol to measure multi-sensory data using a DIC based framework. It has shown that direct-interface to MCU can be easily trained with an aid of artificial intelligence technique for classification of gases. The major advantage of DIC based E-Nose system is that it does not require ADC to acquire sensors analog outputs. To check the distinctness of the system to classify different gases, feature sets were extracted and LDA and PCA are performed, which shows distinctive cluster formation of the four tested gases. FFBP network was also implemented in the µC which shows accuracy up to 98.7 %. The encouraging results open up many possibilities to radically expand the knowledge of direct-interface method to sensor arrays applications. Due to low memory requirement of the adopted method, this intelligent system may find application in various applications.

References

[1] Bengtsson, L. Direct analog-to-microcontroller interfacing. *Sensors and Actuators A: Physical*, 179:105-113, 2012.

[2] Cox, D. Implementing ohmmeter/temperature sensor. *Microchip Technology, Chandler, AZ, Appl. Note AN512*, 1997.

[3] Custodio, A., Pallàs-Areny, R., and Bragós, R. Error analysis and reduction for a simple sensor-microcontroller interface. *IEEE Transactions on Instrumentation and Measurement*, 50(6):1644-1647, 2001.

[4] Gaitán-Pitre, J. E., Gasulla, M., and Pallas-Areny, R. Analysis of a direct interface circuit for capacitive sensors. *IEEE Transactions on Instrumentation and Measurement*, 58(9):2931-2937, 2009.

[5] Gutierrez-Osuna, R. Pattern analysis for machine olfaction: a review. *IEEE Sensors journal*, 2(3):189-202, 2002.

[6] Jordana, J., and Pallas-Areny, R. A simple, efficient interface circuit for piezoresistive pressure sensors. *Sensors and Actuators A: Physical*, 127(1):69-73, 2006.

[7] JSTMicroelectronics, Implementation of sigma-delta ADC with ST7FLUE05/09, in: STMicroelectronics Application Note 1827 [online] (updated 29 February 2008), 2008, from `http://www.st.com/stonline/books/pdf/docs/10304.pdf`

[8] Kokolanski, Z., Jordana, J., Gasulla, M., Dimcev, V., and Reverter, F. Direct inductive sensor-to-microcontroller interface circuit. *Sensors and Actuators A: Physical*, 224:185-191, 2015.

[9] López-Lapeña, O., Serrano-Finetti, E., and Casas, O. Low-power direct resistive sensor-to-microcontroller interfaces. *IEEE Transactions on Instrumentation and Measurement*, 65(1):222-230, 2016.

[10] Nagarajan, P. R., George, B., and Kumar, V. J. Improved single-element resistive sensor-to-microcontroller interface. *IEEE Transactions on Instrumentation and Measurement*, 66(10):2736-2744, 2017.

[11] Peter, D., Baker, B. C., Butler, D., and Darmawaskita, H. Make a Delta-Sigma Converter Using a Microcontroller's Analog Comparator Module. *Microchip Technology Inc., Chandler, Arizona*, 1998.

[12] Reverter, F., Jordana, J., Gasulla, M., and Pallàs-Areny, R. Accuracy and resolution of direct resistive sensor-to-microcontroller interfaces. *Sensors and Actuators A: Physical*, 121(1):78-87, 2005.

[13] Reverter, F., Gasulla, M., and Pallàs-Areny, R. Analysis of power-supply interference effects on direct sensor-to-microcontroller interfaces. *IEEE Transactions on Instrumentation and Measurement*, 56(1):171-177, 2007.

[14] Reverter, F., and Casas, O. Direct interface circuit for capacitive humidity sensors. *Sensors and Actuators A: Physical*, 143(2):315-322, 2008.

[15] Reverter, F., and Casas, O. Interfacing differential resistive sensors to microcontrollers: A direct approach. *IEEE Transactions on Instrumentation and Measurement*, 58(10):3405-3410, 2009.

[16] Reverter, F., and Casas, Ò. Interfacing differential capacitive sensors to microcontrollers: A direct approach. *IEEE Transactions on Instrumentation and Measurement*, 59(10):2763-2769, 2010.

[17] Reverter, F., and Casas, Ò. A microcontroller-based interface circuit for lossy capacitive sensors. *Measurement Science and Technology*, 21(6):065203, 2010.

[18] Sifuentes, E., Casas, O., Reverter, F., and Pallas-Areny, R. Direct interface circuit to linearise resistive sensor bridges. *Sensors and Actuators A: physical*, 147(1):210-215, 2008.

[19] Sifuentes, E., Gonzalez-Landaeta, R., Cota-Ruiz, J., and Reverter, F. Measuring dynamic signals with direct sensor-to-microcontroller interfaces applied to a magnetoresistive sensor. *Sensors*, 17(5):1150, 2017.

[20] Soldera, J. D. B., Espindola, M., and Olmos, A. Implementing a 10-bit Sigma-Delta Analog-to-Digital Converter Using the HC9S08Rx MCU Family Analog Comparator. *Freescale Semiconductor*, 1-22, 2005.

[21] Uyanik, A., and Tinkilic, N. Preparing accurate standard gas mixtures of volatile substances at low concentration levels. *The Chemical Educator*, 4(4):141-143, 1999.

[22] Weber, P., & Windish, C. Build a complete industrial-ADC interface using a microcontroller and a sigma-delta modulator, 2007, from https://www.edn.com/design/analog/4317495/Build-a-complete-industrial-ADC-interface-using-a-microcontroller-and-a-sigma-delta-modulator

[23] Zhang, L., Tian, F., Kadri, C., Pei, G., Li, H., & Pan, L. Gases concentration estimation using heuristics and bio-inspired optimization models for experimental chemical electronic nose. *Sensors and actuators B: Chemical*, 160(1):760-770, 2011.

[24] Zhang, L., Tian, F., Nie, H., Dang, L., Li, G., Ye, Q., and Kadri, C. Classification of multiple indoor air contaminants by an electronic nose and a hybrid support vector machine. *Sensors and Actuators B: Chemical*, 174:114-125, 2012.

[25] Zhang, L., and Tian, F. Performance study of multilayer perceptrons in a low-cost electronic nose. *IEEE Transactions on Instrumentation and Measurement*, 63(7):1670-1679, 2014.